Comput Mech (2008) 41:777–787
DOI 10.1007/s00466-007-0161-2

ORIGINAL PAPER

Fast HdBNM for large-scale thermal analysis of CNT-reinforced composites

Jianming Zhang · Masataka Tanaka

Received: 1 July 2006 / Accepted: 22 December 2006 / Published online: 13 February 2007

Abstract Because of their high thermal conductivities, carbon nanotubes (CNT) have promising potential in development of fundamentally new composites. To study the influence of CNTs distribution on the overall properties of a composite, the modeling of a Representative Volume Element (RVE) including a large number of CNTs that are randomly distributed and oriented is necessary. However, analysis of such a RVE using standard numerical methods faces two severe difficulties, namely the discretization of the geometry and a very large computational scale. In this paper, the first difficulty is alleviated by employing the Hybrid Boundary Node Method (HdBNM), which is a form of the boundary type meshless methods. To overcome the second difficulty, the Fast Multipole Method (FMM) is combined with the HdBNM to solve a simplified mathematical model. RVEs containing various numbers of CNTs with different lengths, shapes and alignments have been analyzed, resulting in valuable insights gained into the thermal behavior of the composite material.

Keywords Hybrid boundary node method · CNT-based composites · Fast multipole method · Heat conduction

J. Zhang (✉)
Department of Engineering Mechanics, Hohai University,
No. 1 Xikang Road, Nanjing 210098, China
e-mail: zhangjianm@gmail.com

M. Tanaka
Faculty of Engineering, Shinshu University,
Nagano 380-8553, Japan

1 Introduction

In recent years, various aspects of the carbon nanotubes (CNT) such as their production, physical properties and possible applications have been intensively investigated [1,2]. Due to their near-perfect nanostructures, the CNTs possess exceptional physical properties such as superior thermal and electrical conductivities and high stiffness and strength. Because of such remarkable properties, the CNT material is an ideal candidate for a wide range of technological applications. One of the most intriguing applications is the use of CNTs, as small volume fraction filler, in nanotube-reinforced polymers. CNT-based composites offer significant improvements to structural properties over those of their base polymers. It has been demonstrated that with only 1% (weight fraction) of CNTs added to a matrix material, the stiffness of a resulting composite may increase as high as between 36 and 42% and the tensile strength up to 25% [3]. In the work of Biercuk et al. [4], samples of industrial epoxy loaded with 1 wt% single-walled CNTs showed a 70% increase in heat conductivity at 40 K. The percentage increase may further rise to 125% at room temperature.

Numerical simulations can aid in the understanding of the relationship between the geometrical characteristic (e.g. nanotube orientation) and the properties of nanocomposites. This may then allow the determination and optimization of different processing method in manufacturing the nanocomposite materials. At the nanoscale level, atomistic or molecular dynamics (MD) may have been the "natural" simulation methods which have provided abundant results needed for understanding the thermal, mechanical and electrical behaviors of nanocomposite [5]. However, due to limitations in current

computing power, such simulations are necessarily limited to single individual pure CNTs or very small scales for CNT-composite such as a representative volume element (RVE) containing only single short CNT. To study how the distribution of CNTs influences the equivalent properties of a composite, a RVE containing a large number of CNTs that are randomly distributed and oriented has to be modeled. This is because a real CNT-composite contains CNTs that are not uniform in size and shape. The CNTs may be straight, twisted and curled or in the form of ropes and their distribution and orientation in the matrix may be nonuniform, unidirectional or random. Even with the most superior computer resources available in the world, computation of such a RVE by MD is almost impossible. Liu et al. [6] has demonstrated that the use of atomistic or molecular dynamics (MD) simulations is inevitable for the analysis of such nanomaterials in order to study the local load transfers, interface properties, or failure modes at the nanoscale. However, for a global analysis of the effects of CNTs configuration on the overall properties of a composite, they suggested a continuum model with the physical behaviors of the composite governed by continuum equations such as Laplace's equation for thermal problems and Lame–Navier equations for elastic problems.

This study seeks to gain useful insights into the thermal properties of CNT-based composites through a numerical simulation based on 3D potential theory. The equivalent heat conductivity of a CNT-based composite is evaluated using a RVE.

For the analysis of a RVE which contains not only one but also many randomly distributed CNTs, the implementation of standard numerical solution techniques such as FEM or BEM may face severe difficulties in the discretization of the solution domain. This is especially so for FEM models in which the meshing of the solid geometries within CNT-reinforced polymers may be tedious and extremely difficult. To alleviate this difficulty, the hybrid boundary node method (HdBNM) may be used [7,8]. By combining a modified functional with the moving least squares (MLS) approximation, the HdBNM is a truly meshless, boundary-only method. We have combined the HdBNM with a multi-domain solver and applied the combined approach to perform some preliminary computations and investigate the influences of the CNT length, curvature and dispersion on the equivalent thermal properties of the composites [9,10].

However, these computations are limited to relatively small scales, as usually only single or several but shorter CNTs were considered. Due to the very thin and slender structure of the CNTs, a large number of nodes are required to discretize them in order to capture the steep gradients. Moreover, in a multi-domain solver, at each node on the interface of a CNT with the host polymer, both temperature and normal flux are unknown. This gives rise to a considerable increase in the total degrees of freedom in the overall system of equations.

Preliminary studies have shown that temperatures within the entire CNT are almost uniform due to the huge difference of heat conductivity between the CNT and the host polymer. Based on this observation, we have proposed a simplified mathematical model in which each CNT is considered as a heat superconductor having uniform temperature within the entire body [11]. As a result, the total number of degrees of freedom is reduced by nearly half. This allows for an increase in the number of CNTs within a RVE that can be analyzed using commonly available computer resources. The simplified model has been rigorously tested and validated using benchmark examples.

Nevertheless, even with the simplified model, both the memory requirements and the computational scale are still of $O(N^2)$ [or worse $O(N^3)$ if a direct solver such as the Gauss elimination technique is used]. Here N stands for the total number of degrees of freedom. To carry out the analysis of a realistic RVE model, an efficient technique for further reducing the computational requirements is necessary. This may be achieved by using the Fast Multipole Method (FMM).

The FMM was introduced by Rokhlin [12], and developed by Greengard [13] as an algorithm for the rapid evaluation of Coulombic interactions in a large-scale ensemble of particles. In their method, multipole moments are used to represent distant particle groups, a local expansion to evaluate the contribution from distant particles in the form of a series, and a hierarchical decomposition of the domain to carry out efficient and systematic grouping of the particles. The FMM reduces both memory size and computational scale from $O(N^2)$ to $O(N)$, thus enabling scientific and engineering computations that were previously impossible.

The FMM has been applied to a variety of computational methods. Application of the FMM for accelerating BEM computation has been investigated by many researchers [14,15]. We have combined the FMM with the HdBNM for large-scale computation of potential problems [16]. In this paper, the FMM techniques are implemented into the HdBNM to solve the simplified model for the simulation of thermal behavior of CNT-based composites. RVEs containing CNTs with different lengths, shapes and alignments have been studied. It is found that some specific alignments may significantly increase the equivalent heat conductivity of the composites.

2 A simplified mathematical model for CNT composites

As mentioned in the introduction, the unusually high thermal conductivity of the CNTs (as compared with the polymer) makes the temperature distribution within an individual CNT almost uniform. This feature allows us to simplify the modeling of the CNT-based composites. In this section, the formulations for the simplified mathematical model are developed, where only single domain, namely the polymer matrix is modeled. Each CNT is treated as a heat superconductor with one constant temperature constrained at its surface. A similar assumption can be found in the rigid-line inclusion model given in [17].

Assume that a RVE contains n CNTs that are distributed in a polymer matrix. It is also assumed that the matrix is continue of linear, isotropic and homogenous materials with given heat conductivities. A steady state heat conduction problem governed by Laplace's equation with proper boundary conditions is considered.

The HdBNM is based on a modified variational principle, in which there are three independent variables, namely:

- temperature within the domain, ϕ;
- boundary temperature, $\tilde{\phi}$;
- boundary normal heat flux, $\tilde{q}$.

Suppose further that N nodes are randomly distributed on the surfaces (including the interfaces with CNTs) of the polymer domain. The temperature within the domain is approximated using fundamental solutions as

$$\phi = \sum_{J=1}^{N} \phi_J^s x_J \tag{1}$$

with the normal heat flux is given by

$$q = -\kappa \sum_{J=1}^{N} \frac{\partial \phi_J^s}{\partial n} x_J \tag{2}$$

where ϕ_J^s is the fundamental solution with the source at a node $\mathbf{s}_J$, κ is the heat conductivity and x_J are unknown parameters. For 3D steady state heat conduction problems, the fundamental solution can be written as

$$\phi_J^s = \frac{1}{\kappa} \frac{1}{4\pi r(Q, \mathbf{s}_J)} \tag{3}$$

where Q is a field point; $r(Q, \mathbf{s}_J)$ is the distance between Q and $\mathbf{s}_J$.

The boundary temperature and normal heat flux are approximated by moving least square (MLS) approximation, that is,

$$\tilde{\phi}(\mathbf{s}) = \sum_{J=1}^{N} \Phi_J(\mathbf{s}) \hat{\phi}_J \tag{4}$$

and

$$\tilde{q}(\mathbf{s}) = \sum_{J=1}^{N} \Phi_J(\mathbf{s}) \hat{q}_J \tag{5}$$

In the foregoing equations, $\Phi_J(\mathbf{s})$ is the shape function of MLS approximation; $\hat{\phi}_J$ and $\hat{q}_J$ are nodal values of temperature and normal flux, respectively.

For the polymer domain, the following set of HdBNM equations can be written:

$$\begin{bmatrix} \boldsymbol{U}_{00} & \boldsymbol{U}_{01} & \cdots & \boldsymbol{U}_{0n} \\ \boldsymbol{U}_{10} & \boldsymbol{U}_{11} & \cdots & \boldsymbol{U}_{1n} \\ \vdots & \vdots & \ddots & \vdots \\ \boldsymbol{U}_{n0} & \boldsymbol{U}_{n1} & \cdots & \boldsymbol{U}_{nn} \end{bmatrix} \begin{Bmatrix} \boldsymbol{x}_0 \\ \boldsymbol{x}_1 \\ \vdots \\ \boldsymbol{x}_n \end{Bmatrix} = \begin{Bmatrix} \boldsymbol{H}_0 \hat{\boldsymbol{\phi}}_0 \\ \boldsymbol{H}_1 \hat{\boldsymbol{\phi}}_1 \\ \vdots \\ \boldsymbol{H}_n \hat{\boldsymbol{\phi}}_n \end{Bmatrix} \tag{6}$$

$$\begin{bmatrix} \boldsymbol{V}_{00} & \boldsymbol{V}_{01} & \cdots & \boldsymbol{V}_{0n} \\ \boldsymbol{V}_{10} & \boldsymbol{V}_{11} & \cdots & \boldsymbol{V}_{1n} \\ \vdots & \vdots & \ddots & \vdots \\ \boldsymbol{V}_{n0} & \boldsymbol{V}_{n1} & \cdots & \boldsymbol{V}_{nn} \end{bmatrix} \begin{Bmatrix} \boldsymbol{x}_0 \\ \boldsymbol{x}_1 \\ \vdots \\ \boldsymbol{x}_n \end{Bmatrix} = \begin{Bmatrix} \boldsymbol{H}_0 \hat{\boldsymbol{q}}_0 \\ \boldsymbol{H}_1 \hat{\boldsymbol{q}}_1 \\ \vdots \\ \boldsymbol{H}_n \hat{\boldsymbol{q}}_n \end{Bmatrix} \tag{7}$$

where subscripts 0 and k $(= 1, \ldots, n)$, stand for quantities exclusively associated with the polymer domain, and quantities associated with its interface with the kth nanotube, respectively. The sub-matrices $[\boldsymbol{U}], [\boldsymbol{V}]$ and $[\boldsymbol{H}]$ are given by

$$U_{IJ} = \int_{\Gamma_I} \phi_J^s v_I(Q) \mathrm{d}\Gamma \tag{8}$$

$$V_{IJ} = -\kappa \int_{\Gamma_I} \frac{\partial \phi_J^s}{\partial n} v_I(Q) \mathrm{d}\Gamma \tag{9}$$

$$H_{IJ} = \int_{\Gamma_I} \Phi_J(\mathbf{s}) v_I(Q) \mathrm{d}\Gamma \tag{10}$$

where Γ_I is a regularly shaped local region around a collocation node $\mathbf{s}_I$, v_I is a weight function and $\mathbf{s}$ is a field point on the boundary. For full details of HdBNM, refer to [8].

By combining Eqs. (6) and (7), we obtain the following equation:

$$\begin{bmatrix} \boldsymbol{A}_{00} & \boldsymbol{A}_{01} & \cdots & \boldsymbol{A}_{0n} \\ \boldsymbol{U}_{10} & \boldsymbol{U}_{11} & \cdots & \boldsymbol{U}_{1n} \\ \vdots & \vdots & \ddots & \vdots \\ \boldsymbol{U}_{n0} & \boldsymbol{U}_{n1} & \cdots & \boldsymbol{U}_{nn} \end{bmatrix} \begin{Bmatrix} \boldsymbol{x}_0 \\ \boldsymbol{x}_1 \\ \vdots \\ \boldsymbol{x}_n \end{Bmatrix} = \begin{Bmatrix} \boldsymbol{H}_0 \boldsymbol{d}_0 \\ \boldsymbol{H}_1 \hat{\boldsymbol{\phi}}_1 \\ \vdots \\ \boldsymbol{H}_n \hat{\boldsymbol{\phi}}_n \end{Bmatrix} \tag{11}$$

where, each row of sub-matrices $[\boldsymbol{A}_{0k}]$, $k = 0, 1, \ldots, n$, is supplied identically from that in $[\boldsymbol{U}_{0k}]$ or $[\boldsymbol{V}_{0k}]$ according to the boundary condition at the corresponding node,

and the corresponding term of $\{\boldsymbol{d}_0\}$ comes from $\left\{\hat{\boldsymbol{\phi}}_0\right\}$ or $\{\hat{\boldsymbol{q}}_0\}$.

Further suppose that m_k nodes are located at the interface of kth nanotube with the polymer with an unknown constant temperature ϕ_c^k, that is,

$$\left\{\hat{\boldsymbol{\phi}}_k\right\} = \{\mathbf{1}\}_k \phi_c^k \tag{12}$$

where $\left\{\hat{\boldsymbol{\phi}}_k\right\}$ are the nodal values of temperature at the interface; $\{\mathbf{1}\}_k$ is a column vector of m_k dimensions with all the elements equal 1. Inserting Eq. (12) into Eq. (11) for all interfaces, the following equation is obtained:

$$\begin{bmatrix} \boldsymbol{A}_{00} & \boldsymbol{A}_{01} & \cdots & \boldsymbol{A}_{0n} & \mathbf{0} & \cdots & \mathbf{0} \\ \boldsymbol{U}_{10} & \boldsymbol{U}_{11} & \cdots & \boldsymbol{U}_{1n} & -\boldsymbol{H}_1\{\mathbf{1}\}_1 & \cdots & \mathbf{0} \\ \vdots & \vdots & \ddots & \vdots & \vdots & \ddots & \vdots \\ \boldsymbol{U}_{n0} & \boldsymbol{U}_{n1} & \cdots & \boldsymbol{U}_{nn} & 0 & \cdots & -\boldsymbol{H}_n\{\mathbf{1}\}_n \end{bmatrix} \begin{Bmatrix} \boldsymbol{x}_0 \\ \boldsymbol{x}_1 \\ \vdots \\ \boldsymbol{x}_n \\ \phi_c^1 \\ \vdots \\ \phi_c^n \end{Bmatrix} = \begin{Bmatrix} \boldsymbol{H}_0\boldsymbol{d}_0 \\ \mathbf{0} \\ \vdots \\ \mathbf{0} \end{Bmatrix} \tag{13}$$

In the above set of equations, there are n (the number of CNTs) more unknowns than the number of equations. This is because we have introduced one additional unknown, i.e. the constant temperature, for each CNT. In order to solve Eq. (13), n more equations are needed. These equations can be obtained from the law of conservation of energy, which states that, for steady state heat conduction, the rate of thermal energy flowing into a CNT must equal that flowing out. Thus, the following integral relation may be imposed on the surface of kth CNT,

$$\int_{C_k} q \mathrm{d}\Gamma = 0 \tag{14}$$

where C_k represents the outer surface of the kth CNT. Substituting Eq. (2) into (14) and omitting the common factor κ, we obtain

$$\sum_{J=1}^{N} \int_{C_k} \frac{\partial \phi_J^s}{\partial n} \mathrm{d}\Gamma \, x_J = 0 \tag{15}$$

In Eq. (15), C_k is a closed surface. The following integral identity holds [18]:

$$\int_{C_k} \frac{\partial \phi_J^s}{\partial n} \mathrm{d}\Gamma = \begin{cases} 1, & \forall \mathbf{s}_J \in C_k \\ 0, & \forall \mathbf{s}_J \notin C_k \end{cases} \tag{16}$$

Therefore, the coefficients in Eq. (15) are either 1 or 0. For nodes located on the surface of the kth CNT, they are 1. Otherwise they are 0. Appending Eq. (15) to Eq. (13) for all CNTs, we obtain the final set of algebraic equations system which may be used to uniquely determine the unknown parameter $\boldsymbol{x}$.

$$\begin{bmatrix} \boldsymbol{A}_{00} & \boldsymbol{A}_{01} & \cdots & \boldsymbol{A}_{0n} & \mathbf{0} & \cdots & \mathbf{0} \\ \boldsymbol{U}_{10} & \boldsymbol{U}_{11} & \cdots & \boldsymbol{U}_{1n} & -\boldsymbol{H}_1\{\mathbf{1}\}_1 & \cdots & \mathbf{0} \\ \mathbf{0} & \{\mathbf{1}\}_1^{\mathrm{T}} & \cdots & \mathbf{0} & 0 & \cdots & 0 \\ \vdots & \vdots & \ddots & \vdots & \vdots & \ddots & \vdots \\ \boldsymbol{U}_{n0} & \boldsymbol{U}_{n1} & \cdots & \boldsymbol{U}_{nn} & \mathbf{0} & \cdots & -\boldsymbol{H}_n\{\mathbf{1}\}_n \\ \mathbf{0} & \mathbf{0} & \cdots & \{\mathbf{1}\}_n^{\mathrm{T}} & 0 & \cdots & 0 \end{bmatrix} \begin{Bmatrix} \boldsymbol{x}_0 \\ \boldsymbol{x}_1 \\ \vdots \\ \boldsymbol{x}_n \\ \phi_c^1 \\ \vdots \\ \phi_c^n \end{Bmatrix} = \begin{Bmatrix} \boldsymbol{H}_0\boldsymbol{d}_0 \\ \mathbf{0} \\ 0 \\ \vdots \\ \mathbf{0} \\ 0 \end{Bmatrix} \tag{17}$$

The total number of degrees of freedom in Eq. (17) is relatively very small when compared with that of a full model (multi-domain solver, see [9]). For each CNT, only one algebraic equation is added. Moreover, as the coefficients of these algebraic equations are either 1 or 0, requiring no tedious computation, both the CPU time and memory usage can be significantly reduced.

The set of Eq. (17) is solved for the unknown parameters $\boldsymbol{x}$, and then, by back-substitution into Eqs. (6) and (7), the boundary unknowns are obtained either on the interfaces or the external boundary surfaces. As demonstrated, the HdBNM is a boundary-only meshless approach. No boundary elements are used for either interpolation or integration purposes. Therefore, the discretization task may be alleviated to a large extent for complicated geometries.

3 Accelerating equation solution by FMM

The size of the coefficient matrix in Eq. (17) is dominated by sub-matrices $[\boldsymbol{A}_{0k}]$ and $[\boldsymbol{U}_{ki}], k = 1, \ldots, n, i = 0, 1, \ldots, n$. Since these sub-matrices are unsymmetrical and fully populated, solving Eq. (17) by an iterative solver requires $O(N^2)$ operations. In this paper, we use the restarted preconditioned GMRES for solving Eq. (17). The most time-consuming aspect of an iterative method when employed for solving a system of linear equations is the matrix-vector product in each iteration step. By taking an iteration vector $\mathbf{x}'$ into account, the product of a row of the coefficient matrix in Eq. (17) and the guess vector $\mathbf{x}'$ can be expressed in terms of one of

the following four sums:

$$\sum_{J=1}^{N}\int_{\Gamma_I}\phi_J^s v_I(Q)x'_J\mathrm{d}\Gamma \tag{18}$$

$$\sum_{J=1}^{N}\int_{\Gamma_I}-\kappa\frac{\partial\phi_J^s}{\partial n}v_I(Q)x'_J\mathrm{d}\Gamma \tag{19}$$

$$\sum_{J=1}^{N}\int_{\Gamma_I}\phi_J^s v_I(Q)x'_J\mathrm{d}\Gamma+\phi'_c\sum_{J}^{m_k}H_{IJ} \tag{20}$$

$$\sum_{J}^{m_k}x'_J \tag{21}$$

The sums in (18) and (19) are related to a node located on the external boundary and prescribed with temperature and normal flux, respectively. The sum in (20) is related to a node located at the interface of the k-th CNT with the polymer domain, and the expression in (21) to the kth uniform temperature constraint.

The computational costs for the second term in sums (20) and (21) are trivial, and thus can be ignored. The summations (18) and (19) are accelerated by FMM with of $O(N)$ operation. The FMM method was first introduced as a fast solution method in astrophysics for simulation of N-body systems in which the interactions between the bodies are gravitational. Because of the computational analogy between the force evaluation for the N-body problem and the matrix–vector multiplication, the FMM is widely employed in conjunction with iterative solvers to accelerate the solutions of elliptic partial differential equations (PDEs) through the boundary integral equation (BIE).

3.1 Cell to cell algorithm

The FMM mainly uses three addition theorems which are briefly explained below.

First addition theorem: Define solid spherical harmonics $R_n^m(\mathbf{r})$ and $S_n^m(\mathbf{r})$ as [14]

$$R_n^m(\mathbf{r})=\frac{1}{(n+m)!}P_n^m(\cos\alpha)\mathrm{e}^{im\beta}r^n$$

$$S_n^m(\mathbf{r})=(n-m)!P_n^m(\cos\alpha)\mathrm{e}^{im\beta}\frac{1}{r^{n+1}}$$

Here (r,α,β) is spherical coordinates of the point $\mathbf{r}$; $P_n^m(\cos\alpha)$ is the associated Lengendre function of integer order m and degree n. Let $\mathbf{r}_1$ and $\mathbf{r}_2$ be two points with spherical coordinates (r_1,α_1,β_1) and (r_2,α_2,β_2), respectively. It follows that

$$\frac{1}{|\mathbf{r_1}-\mathbf{r_2}|}=\begin{cases}\sum_{n=0}^{\infty}\sum_{m=-n}^{n}R_n^m(\mathbf{r}_1)\overline{S_n^m(\mathbf{r}_2)}, & |\mathbf{r}_1|<|\mathbf{r}_2|\\ \sum_{n=0}^{\infty}\sum_{m=-n}^{n}R_n^m(\mathbf{r}_2)\overline{S_n^m(\mathbf{r}_1)}, & |\mathbf{r}_1|>|\mathbf{r}_2|\end{cases} \tag{22}$$

In the above equation, the overhead bar means the complex conjugate of a complex number.

Second addition theorem: If $\mathbf{r}_1$ and $\mathbf{r}_2$ are two vectors such that $|\mathbf{r}_1|>|\mathbf{r}_2|$, then

$$S_n^m(\mathbf{r}_1-\mathbf{r}_2)=\sum_{n'=0}^{\infty}\sum_{m'=-n'}^{n'}\overline{R_{n'}^{m'}(\mathbf{r}_2)}S_{n+n'}^{m+m'}(\mathbf{r}_1) \tag{23}$$

Third addition theorem: If $\mathbf{r}_1$ and $\mathbf{r}_2$ are two arbitrary vectors, then

$$R_n^m(\mathbf{r}_1-\mathbf{r}_2)=\sum_{n'=0}^{n}\sum_{m'=-n'}^{n'}R_{n'}^{m'}(-\mathbf{r}_2)R_{n-n'}^{m-m'}(\mathbf{r}_1) \tag{24}$$

Instead of treating interactions with each of the distant nodes individually, the FMM computes cell–cell interactions. Consider two cells C_a and C_b, which contain N_a and N_b nodes, respectively. The computational complexity of a standard algorithm for the mutual interactions between the two groups is of order $O(N_a\times N_b)$ (see Fig. 1a). In the cell-cell strategy, it is reduced to $O(N_a+N_b)$ (see Fig. 1b).

Substituting Eq. (3) into Eq. (18) and using the first addition theorem (see Fig. 1c), with the summation over the nodes included in C_b, we obtain

$$\sum_{J=1}^{N_b}\int_{\Gamma_I}\phi_J^s v_I(Q)x'_J\mathrm{d}\Gamma=\sum_{n=0}^{\infty}\sum_{m=-n}^{n}\int_{\Gamma_I}\frac{1}{4\pi}\overline{S_n^m}\,\overline{(O_2Q)}v_I(Q)\mathrm{d}\Gamma M_n^m(O_2) \tag{25}$$

where the *coefficients of multipole expansion* $M_n^m(O_2)$ is defined by

$$M_n^m(O_2)=\sum_{J=1}^{N_b}R_n^m\overline{(O_2\mathbf{s}_j)}x'_J \tag{26}$$

Using further the second addition theorem, Eq. (25) becomes

$$\sum_{J=1}^{N_b}\int_{\Gamma_I}\phi_J^s v_I(Q)x'_J\mathrm{d}\Gamma=\sum_{n'=0}^{\infty}\sum_{m'=-n'}^{n'}\int_{\Gamma_I}\frac{1}{4\pi}R_{n'}^{m'}\overline{(O_1Q)}v_I(Q)\mathrm{d}\Gamma L_{n'}^{m'}(O_1) \tag{27}$$

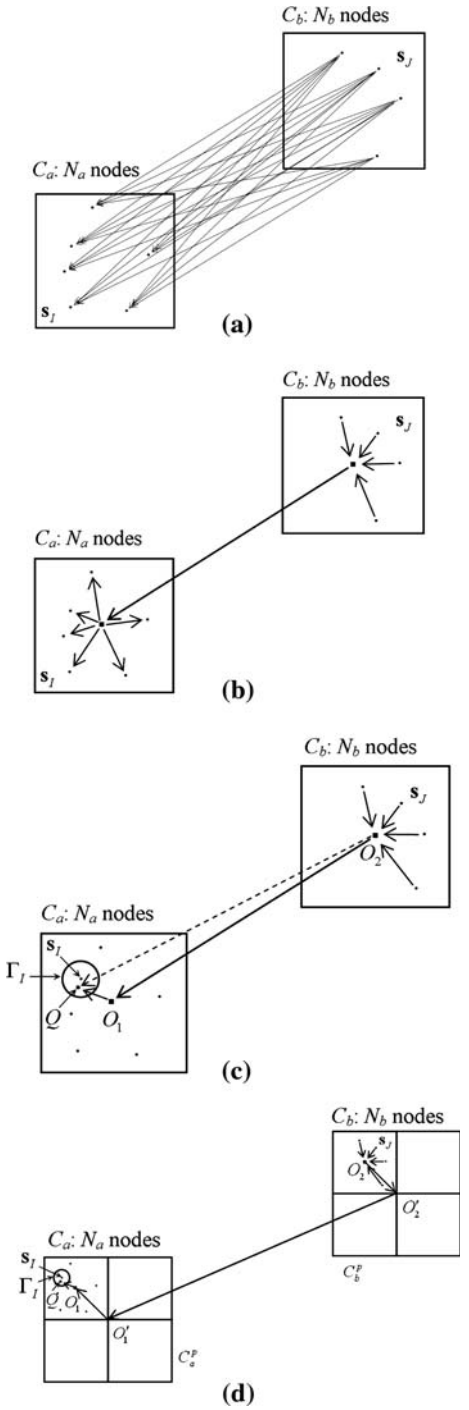

Fig. 1 Interaction between two cells

where the *coefficients of local expansion* $L_{n'}^{m'}(O_1)$ is given by

$$L_{n'}^{m'}(O_1) = \sum_{n=0}^{\infty} \sum_{m=-n}^{n} (-1)^{n'} \overline{S_{n+n'}^{m+m'}(O_1O_2)} M_n^m(Q_2) \quad (28)$$

Equation (28) is known as the *multipole to local* (M2L) translation, as it transforms the *coefficients of multipole expansion* of C_b to the *coefficients of local expansion* of C_a.

Suppose that C_a and C_b are obtained by subdividing other two larger cells C_a^p and C_b^p, known as the parent cells of C_a and C_b, respectively. Assume that C_a^p and C_b^p are still far away from each other (see Fig. 1d). We can then transform the *coefficients of multipole expansion* of C_b to that of C_b^p (M2M) using the third addition theorem, transform the *coefficients of multipole expansion* of C_b^p to *local moments* of C_a^p (M2L), and finally to *coefficients of local expansion* of C_a (L2L) using the third addition theorem again. Therefore, Eq. (28) becomes

$$L_{n'}^{m'}(O_1) = \sum_{n=0}^{\infty} \sum_{m=-n}^{n} R_{n-n'}^{m-m'}(\overline{O_1'O_2}) L_n^m(Q_1') \quad (29)$$

and

$$L_n^m(O_1') = \sum_{n'=0}^{\infty} \sum_{m'=-n'}^{n'} (-1)^n \overline{S_{n+n'}^{m+m'}(O_1'O_2')} M_{n'}^{m'}(Q_2') \quad (30)$$

$$M_{n'}^{m'}(Q_2') = \sum_{n=0}^{\infty} \sum_{m=-n}^{n} R_n^m(\overline{O_2'O_2}) M_{n-n'}^{m-m'}(Q_2) \quad (31)$$

The above process can be recursively repeated until the root cell that contains the entire computational domain. In the above process, the addition theorems are used to separate the source and target points in the fundamental solution and the pair of points in the solid spherical harmonics, so that the *coefficients of multipole expansion* and *local expansion* are related only to the individual cells. Therefore, these coefficients can be calculated independently and can be aggregated into ones to represent temperature due to ever larger groups of nodes. Moreover, once calculated, they can be reused for other cell–cell interactions.

3.2 Tree construction and FMM algorithm

In the previous section, we have described the process of cell–cell interaction. We have seen that the two points in two-point functions can be separated freely by addition theorems. All the resulted coefficients of expansion can be calculated independently. This allows for the freedom to arrange these computations in order to achieve better efficiency. In the FMM, actually, the cell–cell interaction is not performed separately for each pair of well-separated cells. An elaborate algorithm has been designed. This algorithm is facilitated by a tree data structure, which hierarchically decomposes the entire region into cells at different levels.

The standard FMM algorithm uses an oct-tree. The entire computational domain is assumed to lie inside

a cube, which is referred as the root cube at level 0. The oct-tree is constructed by recursively subdividing the cubes into eight sub-cubes by splitting each cube at the geometrically central point. The cubes at level $l+1$ are obtained from cubes at level l, where the eight sub-cubes at level $l+1$ are considered children of the cube at level l. The subdivision continues until cubes contain less than a given number of particles (boundary nodes in HdBNM). If a child cube does not contain any node (that is, it is empty), it is deleted.

With the tree, the FMM consists of two basic steps: *upward pass* and *downwards pass*. During the upward pass, the *coefficients of multipole expansion* are summed from its children using the M2M translation for each non-leaf cube. In the downwards pass, the tree is traversed from the root to leaves to compute the *coefficients of local expansion*. For each Cube C, these coefficients are the sums of two parts. Firstly, the L2L translation collects the coefficients of C's parent. Secondly, the M2L translation collects the *coefficients of multipole expansion* of the cubes which are the children of the neighbors of C's parent but are not adjacent to C (these cubes compose the interaction list of C). Finally, for each leaf, the far interaction, which is evaluated using the *coefficients of local expansion* at this cube is combined with the near interaction evaluated by iterating over all the source nodes in the neighborhood of the leaf cube to obtain the entire sum in Eq. (18).

4 Numerical results

In this section, we first use a numerical example to check the accuracy and efficiency of the FMM, then by employing the algorithms we have developed, study the thermal properties of CNT-based composites.

4.1 Accuracy and efficiency of FMM

The accuracy of FMM is determined by the number of terms, p, used in the multipole expansions. One of the advantages of FMM is that it bounds the error analytically. As we can determine how many terms are required in a multipole expansion to achieve a certain guaranteed level of accuracy, the FMM can be arbitrarily accurate. Because we will study the thermal properties of CNT-based composites by analyzing a Representative Volume Element (RVE) of the composites in the next subsection, we use a similar RVE embedded with a number of cavities of curved tube-like shapes to examine the accuracy of the FMM. Figure 2 shows the geometry and dimensions. As there is no analytical solution existing for the simplified model, we consider a potential

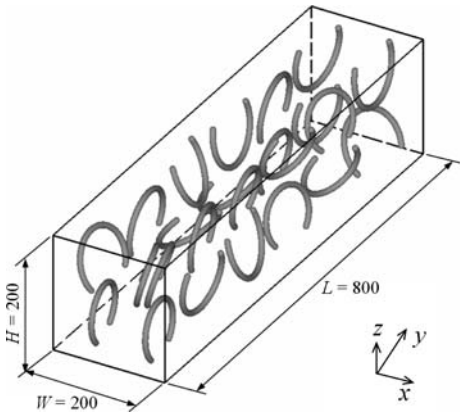

Fig. 2 Dimensions of a nanoscale RVE

problem, and impose Dirichlet boundary condition on all the surfaces, including that of the cavities, according to the following exact solution:

$$\phi = x^3 + y^3 + z^3 - 3yx^2 - 3xz^2 - 3zy^2 \tag{32}$$

Then solve the problem using Eqs. (6) and (7). This set up cannot actually check the accuracy of the simplified model combined with FMM but the FMM, only. The simplified mathematical model has been rigorously validated in [11]. The relative error is evaluated over all the boundary nodes using a 'global' L_2 norm error defined as

$$e = \frac{1}{|q|_{\max}} \sqrt{\frac{1}{N}\sum_{i=1}^{N} \left(q_i^{(e)} - q_i^{(n)}\right)^2} \tag{33}$$

where $|q|_{\max}$ is the maximum nodal value of normal flux, the superscripts (e) and (n) refer to the exact and numerical solutions, respectively.

We have performed computations for four sets of node arrangements, namely 24,071, 47,032, 94,728 and 187,552 nodes uniformly distributed on the inner and outer surfaces of the domain. We truncate all the infinite expansions after $p = 10$, set the maximum number of boundary nodes in a leaf box to be 60, and terminate the iteration when the relative error norm is less than 10^{-5}. All the computations, including that will be presented in the next subsection, are performed on a desktop computer with an Intel(R) Pentium(R) 4 CPU (1.99 GHz).

The relative errors of normal flux computed by Eq. (33) are presented in Fig. 3 as a function of the number of nodes used in the computations. With an increasing number of nodes, higher accuracy is obtained. The run time for solving the system equation is plotted against the number of nodes in Fig. 4, which clearly shows a

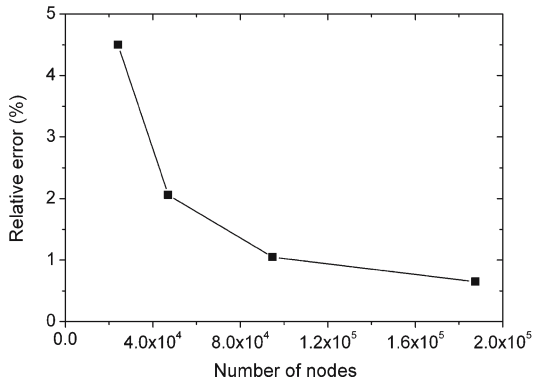

Fig. 3 Relative error for normal flux

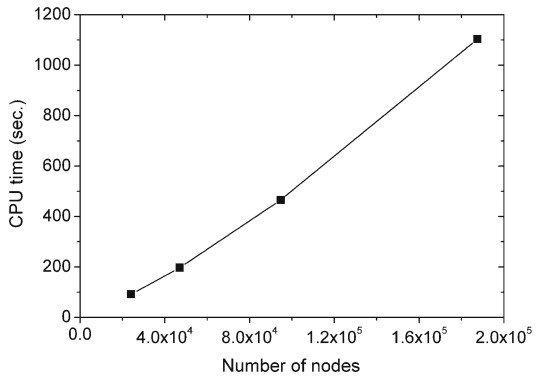

Fig. 4 CPU seconds for solving system equation

nearly linear complexity of the developed algorithm. The high accuracy and efficiency for this example suggests that the proposed formulation and its FMM implementation are correct and effective. This example also demonstrates that the proposed method is capable of performing large-scale computations, because without FMM, the largest number of node of a problem that can be solved by the HdBNM is about 5,000, only. In the next subsection, we will employ it for advanced analysis of the CNT-based composites.

4.2 Study on the thermal behavior of CNT-based composites

In this subsection, we use a RVE to study the CNT-based composites for their thermal properties. The outer dimensions of the RVE are kept the same as the one used in the previous subsection (see Fig. 2), but we will change the number and shape of the CNTs that are embedded in the RVE. Based on the simplified mathematical model, the CNTs are treated as cavities of which the surfaces are identical to the outer surfaces of the CNTs, and a constant temperature is constrained at each cavity. The heat conductivity, κ^p, used for the polymer (polycarbonate) is 0.37 W/m K, and for CNT 1,750 W/m K. Uniform temperatures of 300 and 200 K are imposed at the two square faces, respectively, and heat flux free at other four rectangular faces. These boundary conditions allow us to estimate the equivalent heat conductivity of the composite in the axial direction. Using Fourier's law, the formula for the equivalent heat conductivity can be written as

$$\kappa = -\frac{qL}{\Delta\phi} \tag{34}$$

where κ represents the heat conductivity; q is the average value of normal flux at the two end face, obtained by HdBNM; L is the length of the RVE in the axial direction and $\Delta\phi$ the temperature difference between the two square faces.

Figure 5 gives 7 sets of 3 RVEs. The radii of CNTs ($R = 5$ nm) are kept constant, while their lengths and shapes, together with the number of CNTs and their alignments, varies for different cases. The locations and orientations of the CNTs are "random". The word random is quoted because the variations of location and orientation are limited to a small extent that each CNT remains in a local box that includes the CNT to avoid contact of the CNTs. Each set contains CNTs of a specific shape and alignment. Specifically, sets 1 (RVE (1) to (3)), 2 (RVE (4) to (6)) and 3 (RVE (7) to (9)) deal with CNTs of "C" shape, set 4 (RVE (10) to (12)) sinusoidal shape, sets 5 (RVE (13) to (15)) and 6 (RVE (16) to (18)) spiral shape and set 7 (RVE (19) to (21)) straight CNTs. Within each set, the first RVE contains a small number but long CNTs. From the first to the third, the number of CNTs increases while the lengths of CNTs decrease.

Results of our experiments are summarized in Table 1. The first and second columns of the table are the set number and the RVE number; the third, fourth and fifth columns list the average length in nanometer, the total number and the volume fraction of the CNTs. In the sixth and seventh columns, the total number of nodes used for the simulation and the equivalent heat conductivity (in W/m K) are listed, respectively. To assess the enhancement effectiveness, we use as a criterion the ratio of the equivalent heat conductivity to the volume percentage of CNT. The ratio is presented in the eighth column of the table. The ninth column lists the CPU times in second used for solving the system equation.

From the results it is seen that, within each set, both the equivalent heat conductivity and the ratios κ/v of the first RVE are significantly larger than that of the second and third RVEs, although the volume fraction is relatively much smaller. This suggests that CNT length is a decisive factor for the enhanced thermal property of the composite, while the volume fraction of CNT is much less important. The most effective way to increase

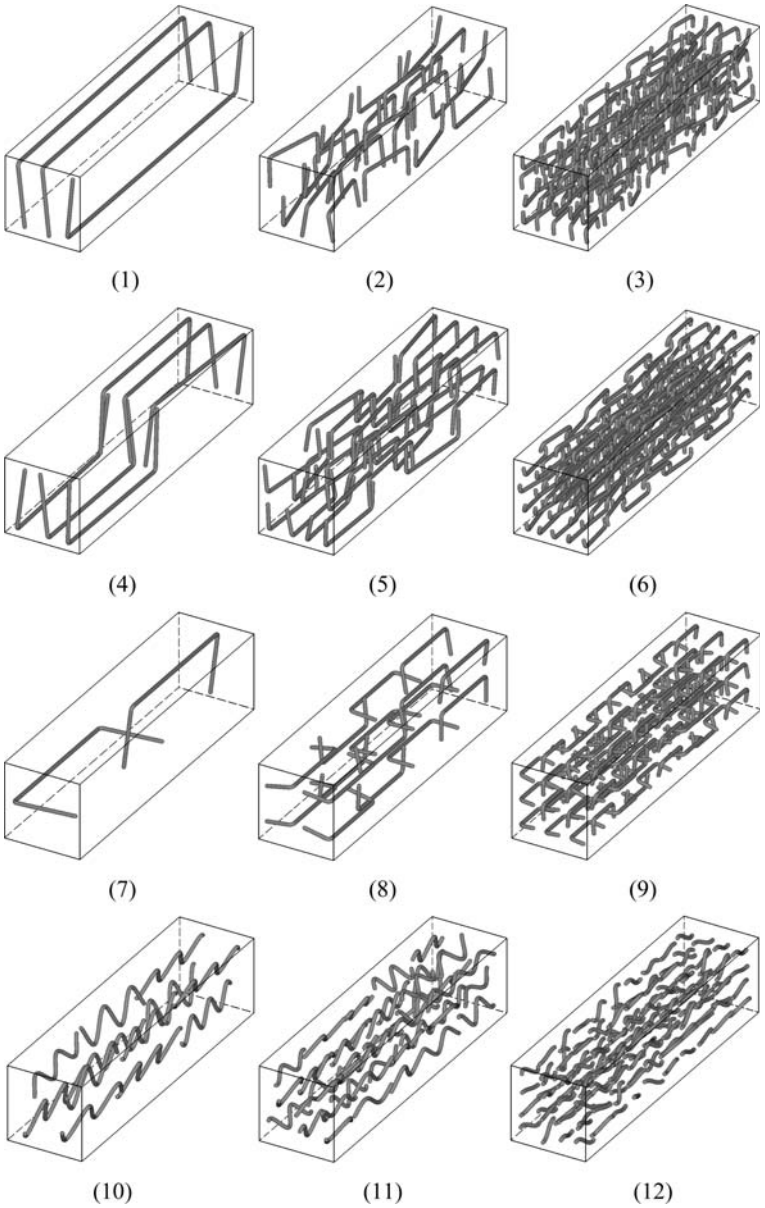

Fig. 5 RVEs with various alignments of CNTs

the heat conductivity of the composite is to use longer CNTs.

It is also noticed that the shape of CNTs strongly affects the overall properties of the composites. Comparing the results of different sets, we found that the "C" shape is the best.

The CPU seconds listed in the ninth column of Table 1 is plotted in Fig. 6 against the number of nodes. Again, we see that the time complexity of the FMM is approximately linear with respect to the number of nodes.

5 Concluding remarks

In this paper, formulations of a simplified mathematical model for simulation of thermal behaviors of CNT-based composites are presented. The model provides remarkable improvement in computational efficiency. The FMM is employed to further reduce the computational costs. Numerical examples have demonstrated that the fast HdBNM is an effective algorithm and has promising applications in large-scale analyses of CNT composites, especially when the CNTs involved have complex geometries.

A variety of RVEs containing different numbers of CNTs have been studied in an attempt to investigate the influence of CNT length, distribution, orientation and volume fraction on the overall thermal properties of the composites. We found that all the above factors have strong impact on the overall properties of the composites. However the average length of the CNTs is

Fig. 5 continued

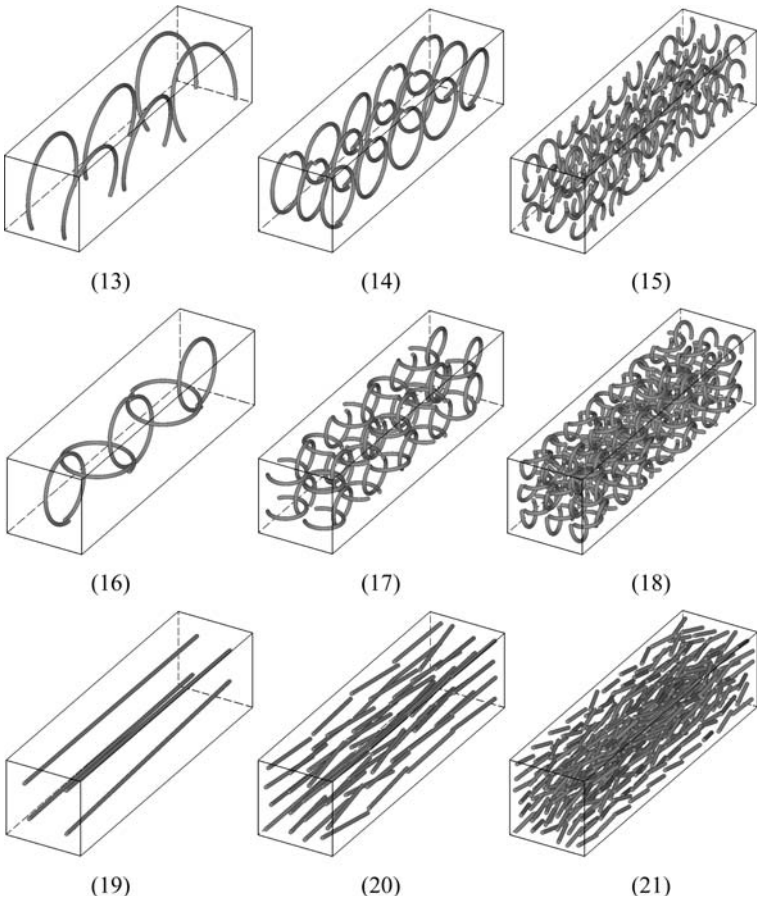

Table 1 Numerical results obtained for RVEs

Set no.	RVE no.	Average length	Number of CNTs	Fraction v (%)	Number of nodes	k	k/v	Run time
	(1)	1117.3	3	0.59	40,614	8.472	1435.9	232
1	(2)	312.3	24	1.09	54,320	2.432	223.1	1341
	(3)	139.8	160	3.78	110,102	1.356	35.9	5865
	(4)	728.9	6	0.61	46,824	5.010	821.4	389
2	(5)	342.7	32	1.77	71,908	3.937	222.4	2042
	(6)	149.5	160	5.07	134,756	2.833	55.9	6880
	(7)	728.9	2	0.28	40,816	1.773	633.1	201
3	(8)	342.7	16	1.11	68,563	2.086	187.9	2447
	(9)	162.9	90	2.97	147,496	1.745	58.8	8320
	(10)	437.7	12	1.29	50,148	1.186	91.9	1591
4	(11)	205.1	45	2.23	66,740	1.097	49.2	2703
	(12)	80.2	160	3.06	88,962	0.760	24.8	5708
	(13)	516.6	6	0.76	39,780	1.551	205.5	343
5	(14)	462.5	15	1.69	51,006	1.184	70.1	1321
	(15)	149.1	90	3.17	72,876	0.917	28.9	3237
	(16)	537.9	5	0.66	38,556	0.796	121.3	416
6	(17)	239.2	40	2.31	59,556	1.094	47.34	2591
	(18)	149.6	135	4.84	93,936	1.709	35.31	4266
	(19)	790.0	4	0.77	39,852	2.990	387.4	581
7	(20)	194.7	64	2.99	68,954	1.790	59.85	4234
	(21)	77.0	360	6.33	128,592	1.204	19.02	9504

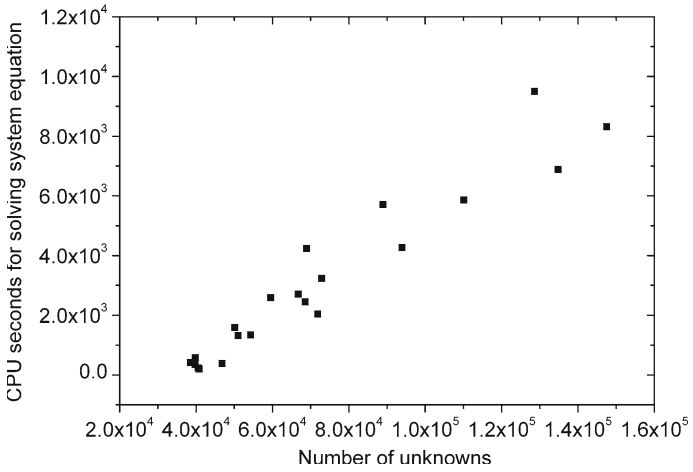

Fig. 6 CPU seconds for solving system equation

substantially decisive for enhancing the thermal properties of the composite, while the volume (or weight) fraction of CNT is less important. For a specific length of CNTs, the "C" shape is suggested to be the most effective shape for thermal property enhancement.

Acknowledgments Authors gratefully acknowledge support of *Japan Society for the Promotion of Science* and Shinshu University. Parts of this work were financially supported by the Grant-in-Aid for JSPS Fellows No. 17_05075.

References

1. Endo M, Kim YA, Hayashi T, Nishimura K, Matushita T, Miyashita K, Dresselhaus MS (2001) Vapor-grown carbon fibers: basic properties and their battery applications. Carbon 39:1287–1297
2. Endo M, Kim YA, Nishimura K, Matushita T, Hayashi T (2001) From vapor-grown carbon fibers (VGCFs) to carbon nanotubes. In: Biro LP, Bernardo CA, Tibbetts GG, Lambin P (eds) Carbon filaments and nanotubes: common origins, differing applications. NATO Science Series E: Applied Sciences, Kluwer, pp 51–61
3. Qian D, Dickey EC, Andrews R, Rantell T (2000) Load transfer and deformation mechanisms in carbon CNT polystyrene composites. Appl Phys Lett 76:2868–2870
4. Biercuk MJ, Llaguno MC, Radosavljevic M, Hyun JK, Johnson AT, Fischer JE (2002) Carbon nanotube composites for thermal management. Appl Phys Lett 80:2767–2769
5. Liu YJ, Chen XL (2003) Evaluations of the effective material properties of carbon CNT-based composites using a nanoscale representative volume element. Mech Mater 35:69–81
6. Liu YJ, Nishimura N, Otani Y (2005) Large-scale modeling of carbon-nanotube composites by a fast multipole boundary element method. Comput Mater Sci 34:173–187
7. Zhang JM, Yao ZH, Li H (2002) A hybrid boundary node method. Int J Numer Methods Eng 53:751–763
8. Zhang JM, Tanaka Masa, Matsumoto T (2004) Meshless analysis of potential problems in three dimensions with the hybrid boundary node method. Int J Numer Methods Eng 59:1147–1160.
9. Zhang JM, Tanaka Masa, Matsumoto T, Guzik A (2004) Heat conduction analysis in bodies containing thin-walled structures by means of HdBNM with an application to CNT-based composites. JSME Int J Series A Solid Mech Mater Eng 47:181–188
10. Tanaka Masa, Zhang JM, Matsumoto T (2003) Multi-domain HdBNM for prediction of thermal properties of CNT composites. In: Honma T, Tanaka Masa (eds) Proceedings of the first Asia-Pacific international conference on computational methods in engineering. ICOME, Sapporo, Japan, pp 3–12
11. Zhang JM, Tanaka Masa, Matsumoto T (2004) A simplified approach for heat conduction analysis of CNT-based nanocomposites. Comput Methods Appl Mech Eng 193:5597–5609
12. Rokhlin V (1985) Rapid solution of integral equations of classical potential theory. J Comput Phys 60:187–207
13. Greengard L, Rokhlin V (1987) A fast algorithm for particles simulations. J Comput Phys 73:325–348
14. Yoshida K, Nishimura N, Kobayashi S (2001) Application of fast multipole Galerkin boundary integral equation method to elastostatic crack problems in 3D. Int J Numer Methods Eng 50:525–547
15. Nishida T, Hayami K (1997) Application of the fast multipole method to the 3D BEM analysis of electron guns. In: Marchettia M, Brebbia CA, Aliabadi MH (eds) Boundary elements XIX (Computational Mechanics Publications), pp 613–622
16. Zhang JM, Tanaka Masa, Endo M (2005) The hybrid boundary node method accelerated by fast multipole method for 3D potential problems. Int J Numer Methods Eng 63:660–680
17. Liu YJ, Nishimura N, Otani Y, Takahashi T, Chen XL, Munakata H (2005) A fast boundary element method for the analysis of fiber-reinforced composites based on a rigid-inclusion model. J Appl Mech 72:115–128
18. Liu YJ, Rudolphi TJ (1999) New identities for fundamental solutions and their applications to non-singular boundary element formulations. Comput Mech 24:286–292